Engineering Structures 283 (2023) 115896

Contents lists available at ScienceDirect

Engineering Structures

journal homepage: www.elsevier.com/locate/engstruct

Experimental investigation of mechanically laminated straight or curved-and-tapered bamboo-concrete T-beams

Yu Deng [a], Yuxi Hao [a], Ahmed Mohamed [b,*], Simon H.F. Wong [c], Yunchao Tang [d], Terry Y.P. Yuen [e], Piti Sukontasukkul [f], Minhe Shen [a,b], Nirodha Fernando [b], Ruth Saint [b], Hexin Zhang [b,*]

[a] School of Civil Engineering and Architecture, Guangxi University of Science and Technology, Liuzhou 545006. China
[b] School of Computing, Engineering and the Built Environment, Edinburgh Napier University, 10 Colinton Road, Edinburgh EH10 5DT, Scotland, UK
[c] Faculty of Science and Technology, Technological Higher Education Institute of Hong Kong, 20A Tsing Yi Road, Tsing Yi Island, New Territories, Hong Kong
[d] College of Urban Construction, Zhongkai University of Agriculture and Engineering, Guangzhou 510225, China
[e] Department of Civil Engineering, National Yang Ming Chiao Tung University, Hsinchu 30010, Taiwan
[f] Construction and Building Materials Research Center, Department of Civil Engineering, King Mongkut's University of Technology North Bangkok, Thailand

ARTICLE INFO

Keywords:
Curved beam
Laminated bamboo-concrete
Composite structure
Bamboo structure
Interface slip

ABSTRACT

This study echoes the rising demand for bio-based material in concrete composite structures in the race to accelerate carbon neutrality in construction. Noticing that most previous studies are focused on straight timber or engineered bamboo-to-concrete composite beams, this study developed straight or curved-and-tapered mechanically laminated bamboo-concrete (LBC) T-beams. Six layers of 26 mm thick laminated bamboo panels were glue laminated together to form the bamboo beams. The curved bamboo beams have three different rises of arch: 50 mm, 100 mm and 150 mm. All specimen beams were tested by four-point bending tests to evaluate their structural performances of the curved and straight LBC T-beams. To monitor the flange-to-web interface shear transfer, a novel interface shear slip calibration method that captures the longitudinal after-slip strain redistribution was developed and validated by strain gauge measurements. This study also highlights the interlayer shear bonding strength of laminated bamboo as the thresholding parameter that determines the composite beams' overall flexural strength, evidenced by detailed failure mode analysis. The proposed interface shear slip calibration method can be extended to the other types of shear connectors such as screws, nails, shear plates and notched connections.

1. Introduction

Timber-concrete composite (TCC) systems have become more popular in modern construction in the past decade and their popularity has accelerated in recent years due to the net-zero campaign. These engineered concrete-wood products are usually used for structural elements, which are mainly subjected to bending load, from simple floor systems to long-span bridges [1]. An increasing number of TCC structures have been applied in the refurbishment of existing timber floors, construction of new floors, or as a deck for timber bridges all around the world [2]. The growing demands from the industry have also attracted increasing research interest in this area and its relevant supporting technologies in recent years [3–12]. However, growing concerns associated with deforestation's environmental and ecological impact highlight the need for alternatives to traditional wood materials.

In the search for non-timber forest products to substitute for wood, bamboo, as a fast-growing giant grass, has emerged as a leading candidate. In particular, it is now widely recognised that bamboo may be an ideal replacement for wood in several applications owing to its comparable strength to modern structural materials, easy processing, and rapid growth compared to common trees. Engineered bamboo products, laminated bamboo and bamboo scrimber (densified bamboo product) being two of the most popular forms, have become increasingly popular in many applications including construction, which has attracted intensive research attention recently [13–17].

One form of engineered bamboo in construction is engineered bamboo-concrete composite beams. Compared to timber, engineered bamboo products have better mechanical strength [18], better ductility

* Corresponding authors.
E-mail addresses: A.Mohamed2@napier.ac.uk (A. Mohamed), j.zhang@napier.ac.uk (H. Zhang).

https://doi.org/10.1016/j.engstruct.2023.115896
Received 2 November 2022; Received in revised form 19 February 2023; Accepted 23 February 2023
Available online 4 March 2023
0141-0296/

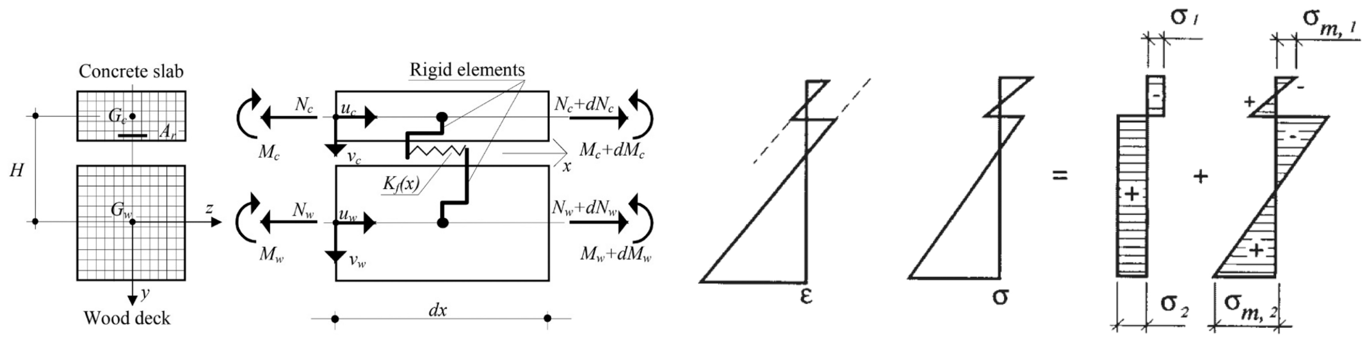

(a) Rigid blocks and spring analogy [32]

(b) Strain and stress distributions [33]

Fig. 1. Rigid block and spring analogy model [32,33,48].

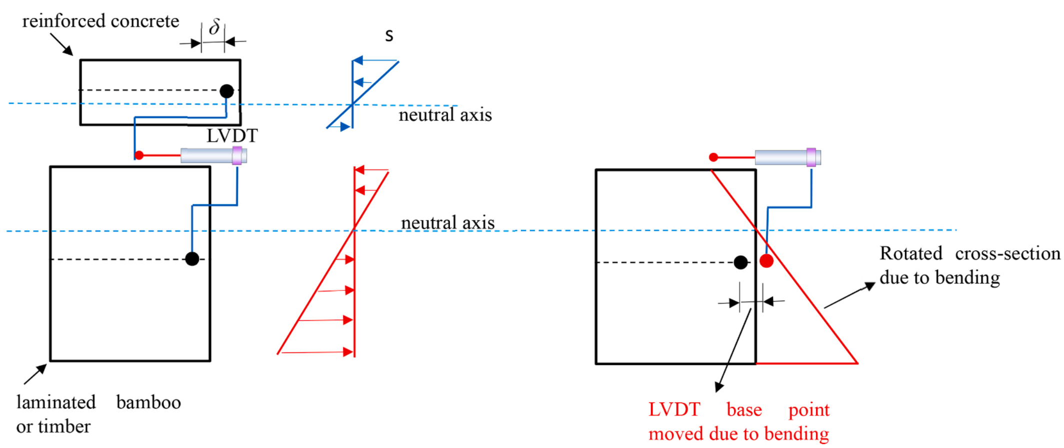

Fig. 2. Concrete to timber/laminated bamboo slip monitoring.

[15], and remarkable mouldability under appropriate thermal-mechanical conditions [19], making them suitable candidates to replace timber in TCC structures. However, most previous studies focus on engineered bamboo-concrete beams' simplest shape/format, i.e., straight rectangular or T-beams [20–26]. To the authors' best knowledge, no study has focused on curved engineered bamboo-concrete composite structures, despite curved structural members inevitably being adopted more frequently due to the necessity for contemporary architectural expressions. Given the growing popularity of TCC structures and the accelerating race to search for non-timber forest products, laminated bamboo is becoming one of the best timber alternatives for developing bio-based materials and concrete composite for straight and curved structural members. Laminated bamboo has many advantages and is considered a better candidate than timber when constructing structures with curved and more complex shapes due to its mouldability and the customisability the production process.

This study echoes the rising demand for curved bio-based material and concrete composite structures, focusing on the development of unique curved laminated bamboo-concrete (LBC) composite beams. The structural performance of the curved and straight LBC beams, including the failure modes, flexural properties, and strain distribution, were comprehensively investigated using the four-point bending test. The results could provide practical guidance for improving the manufacturing and design of the LBC composite beams. Another key objective of this study is to develop a novel and proper flange-to-web interface shear slip calibration method. This method calibrates interface shear slip at the structural member level and validates with purpose-mounted strain gauges. The proposed method is completely different from the widely used small specimen push-out tests [27–31], where the real stress status in full-scale TCC or LBC beams may not be accurately replicated. The difference in background stress/strain status also resulted in conflict with fundamental assumptions when applying the results from the small shear push-out tests to the commonly adopted spring-rigid block analogy [32–34].

According to the spring-rigid block analogy, as shown in Fig. 1, in the middle pure bending section of a TCC or LBC beam, the shear force should be zero; thus, the spring should have no force in this section. There should have no interface shear slip between these two components. However, our test results suggested the opposite. Furthermore, according to the spring-rigid block model, the slip should be measured as the geometrical centre to centre to satisfy the uniformly distributed axial forces assumption. However, as the concrete (if considering the reinforcing inside) and laminated bamboo or timber are not isotropic materials, the neutral axes of each component may not pass through the geometrical centres. In this case, as shown in Fig. 2, the linear variable differential transformer (LVDT) mounted on the centres of the concrete and laminated bamboo or timber component will move along the longitudinal direction due to the bending. It makes it very hard to validate the load-slip model obtained from the push-out tests with the concrete to timber or laminated bamboo interface shear slip measurement in a full-scale structural member test due to the different background stress statuses in these two different types of tests.

An alternative setup for shear connection slip measurement is to mount the LVDTs next to the contact surfaces of the concrete to laminated bamboo/timber [21,35], but the measurement also included the effect of bending. As the push-out test creates shear only condition but stress condition between the interface of a four-point bending scenario is much more complicated to be correlated to the push-out test result

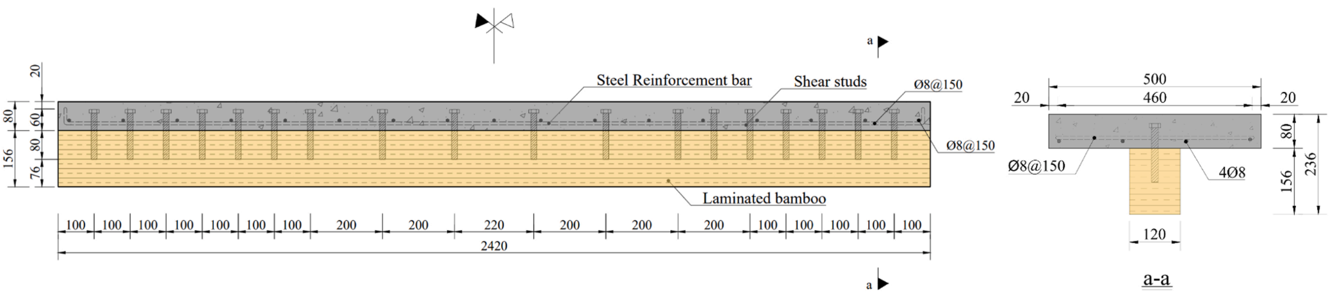

(a) Design details of the straight LBC composite beam - BCC-0

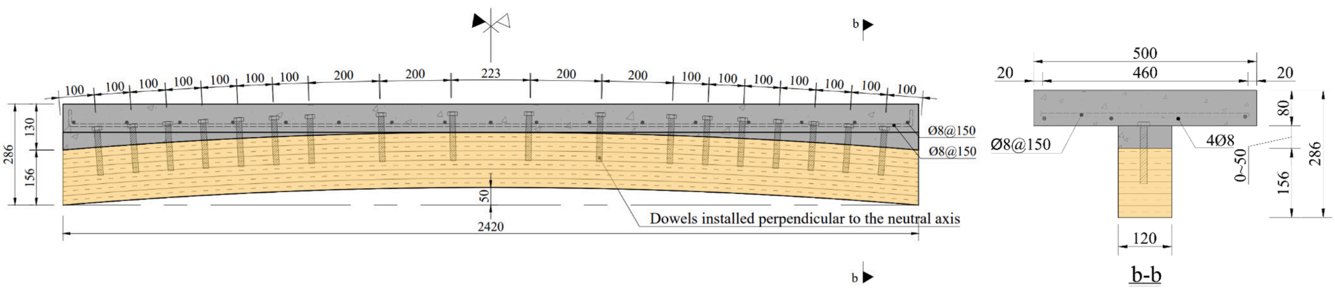

(b) Design details of the type 1 curved LBC composite beam - BCC-1

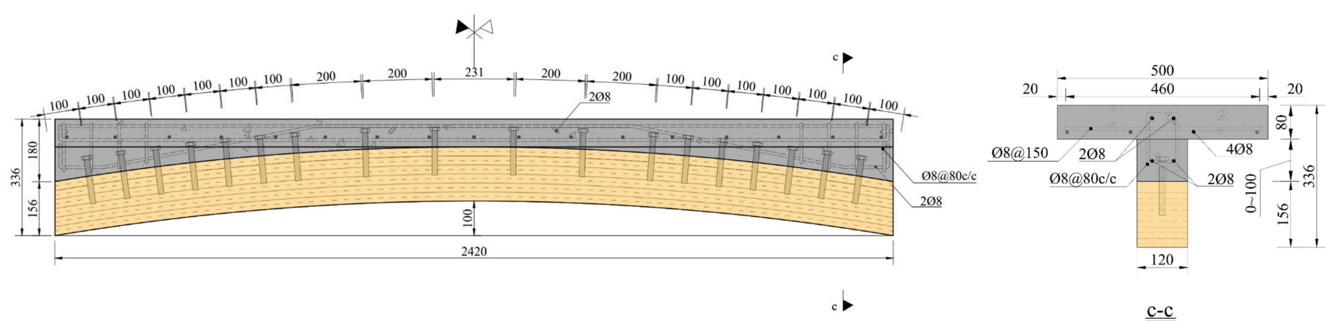

(c) Design details of the type 2 curved LBC composite beam - BCC-2

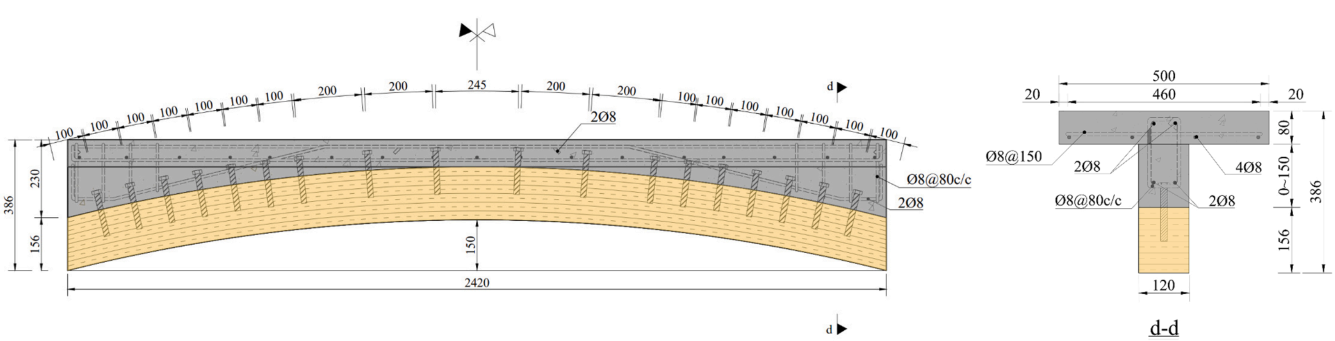

(d) Design details of the type 3 curved LBC composite beam - BCC-3

Fig. 3. Detailed CAD drawings of four types of specimen beams.

Table 1
Dimensions of the four types of specimens.

Type of Specimen	Specimen ID	Length of composite beam [mm]	Cross-section size of laminated bamboo component (width×height) [mm]	Concrete slab size (width×thickness) [mm]	Rise of Arch [mm]
	BCC-0a、b	2420	120 × 156	500 × 80	0
	BCC-1a、b	2420	120 × 156	500 × 80	50
	BCC-2a、b	2420	120 × 156	500 × 80	100
	BCC-3a、b	2420	120 × 156	500 × 80	150

easily. The study of interlayer slip in timber structures can be traced back to the mid-twentieth century [36]. Smith [37] developed series-type solutions for determining stresses and deflections for two- and three-piece built-up timber beams [38] for which connections between layers are semi-rigid. The predictions from the proposed theory were in good agreement with experimental results. Latham et al. developed a new finite element for two-layer plates with built-in interlayer slip [39]. However, there is no previous study focused on LBC beams. In this study, the performance of the shear connectors is converted to an average index of concrete to laminated bamboo interface shear slip, scored by the strain difference at two sides of the interface. The strain difference is then used to profile the stress difference, from which, the cross-section stress distribution can be calculated as well.

In this paper, Sections 2–4 focus on experimentally investigating the structural performance of curved or straight LBC composite beams. Then, based on the experimental results, Section 5 focuses on developing the flange-to-web interface calibration method for quantifying concrete to laminated bamboo interface shear slip.

2. Design of test specimens and fabrication

2.1. Overall experimental plan

The main objectives of this study are: 1) to reveal the main different structural behaviours between the curved and straight LBC composite beams; 2) to investigate the impact of the curvatures on the structural performances of the LBC composite beams; and 3) to summarise and classify the failure mode to understand the failure mechanisms of LBC composite beams. To achieve these objectives, a detailed experimental plan with eight LBC beams was designed and implemented in this study. Among these eight beams, two are straight beams with a straight laminated bamboo component of 120 mm × 156 mm rectangular cross-section. The concrete layer is a 500 mm wide, 80 mm thick flat plate, connected by M16 bolts [40] as the shear studs to form a straight LBC composite beam. More details are specified in Fig. 3(a). The other six beams are curved LBC beams with different arch heights of 50 mm, 100 mm, and 150 mm. The top concrete slabs are flat with the same dimensions as the straight beams. The gaps between the top surface of the curved laminated bamboo beam and the bottom surface of the concrete slab are infilled with wedge-shaped concrete cast monolithically. The reinforcement detailing and other design information can be found in Fig. 3(b)-(d). A completed summary of the dimensions of these four types of specimens is shown in Table 1.

2.2. Fabrication of the specimen beams

2.2.1. Fabrication of the laminated bamboo arch component

The laminated bamboo arch components were fabricated in an industrial facility with a customised production process. The process started with harvesting bamboo (*Phyllostachys edulis*) culms from Jiangxi province in China at the age of four. The bamboo culms were then cut into 2.5 m ~ 2.8 m long sections based on their node locations. After initial inspection for exterior defects and visual grading based on the diameter and wall thickness, the bamboo poles were ready for processing, as shown in Fig. 4(a). The round bamboo culms were then split into long strips with arc-shape cross-sections, and the outer green skin (epidermis) and inner yellow layer (pith ring) were planed off to produce strips with 6 mm to 10 mm thickness and an 18 mm high rectangular cross-section as shown in Fig. 4(b). These roughly trimmed strips were then thermally treated with 110 °C to 120 °C steam for one hour and then kiln dried at 30 °C to 45 °C for two days until the moisture content dropped to 8% to 12%. The treated bamboo strips, shown in Fig. 4(c), were trimmed to 2.5 m in length, as shown in Fig. 4(d). The long side surfaces were fine-planed to provide a fresh gluing surface for edgewise lamination. Around 18 bamboo strips were grouped to give a minimum 120 mm width, and were then glued in a panel-making machine using phenol-resorcinol adhesive, as shown in Fig. 4(e). The panels were pressed with 1.0 MPa vertical and 1.2 MPa side pressure for a period of 25 min at a temperature of approximately 650 °C as shown in Fig. 4(f). Each of these 18 mm thick, 120 mm + wide panels was sawn into three equal slices, as shown in Fig. 4 (g)-(h). The thinner and more flexible sliced panels can much more easily be moulded into curved laminated bamboo lumber. Each slice was sanded to 2440 mm × 120 mm × 5.2 mm in size before being moulded into curved laminated bamboo lumber. Several pairs of purpose-built arc-shaped mould inserts with different radians were used to produce the curved laminated bamboo component. The freshly planed laminated bamboo thin slices were hand-brushed with the fully mixed low foaming D4 Polyurethane structural adhesive from Akzo Nobel (Fig. 4(i)), and then a total of 30 layers of thin laminated bamboo slices were stacked together between a pair of curved inserts and pressed for 12 h using the hydraulic press machine as shown in Fig. 4(j).

2.2.2. Shear stud installation

M16, Grade 8.8 high-strength bolts with a total length of 140 mm were used as the shear studs in this study. The mechanical properties of the shear studs are specified in Table 2; they were installed on the top surfaces of the straight or curved laminated bamboo components. The location of each stud is shown in the detailed design drawing of each specimen (Fig. 3). To install the shear studs, 80 mm deep holes with an 18 mm diameter were drilled at designed positions on the top centre line of the laminated bamboo components and the completed holes were blasted with an air gun to remove any drill dust. The shear stud adhesive used in this study was two parts E-44 epoxy resin manufactured by Shenzhen Mingde Chemical Engineering Ltd. The mix ratio of the two parts was 100:40 in weight. The shear studs and pre-drilled holes were

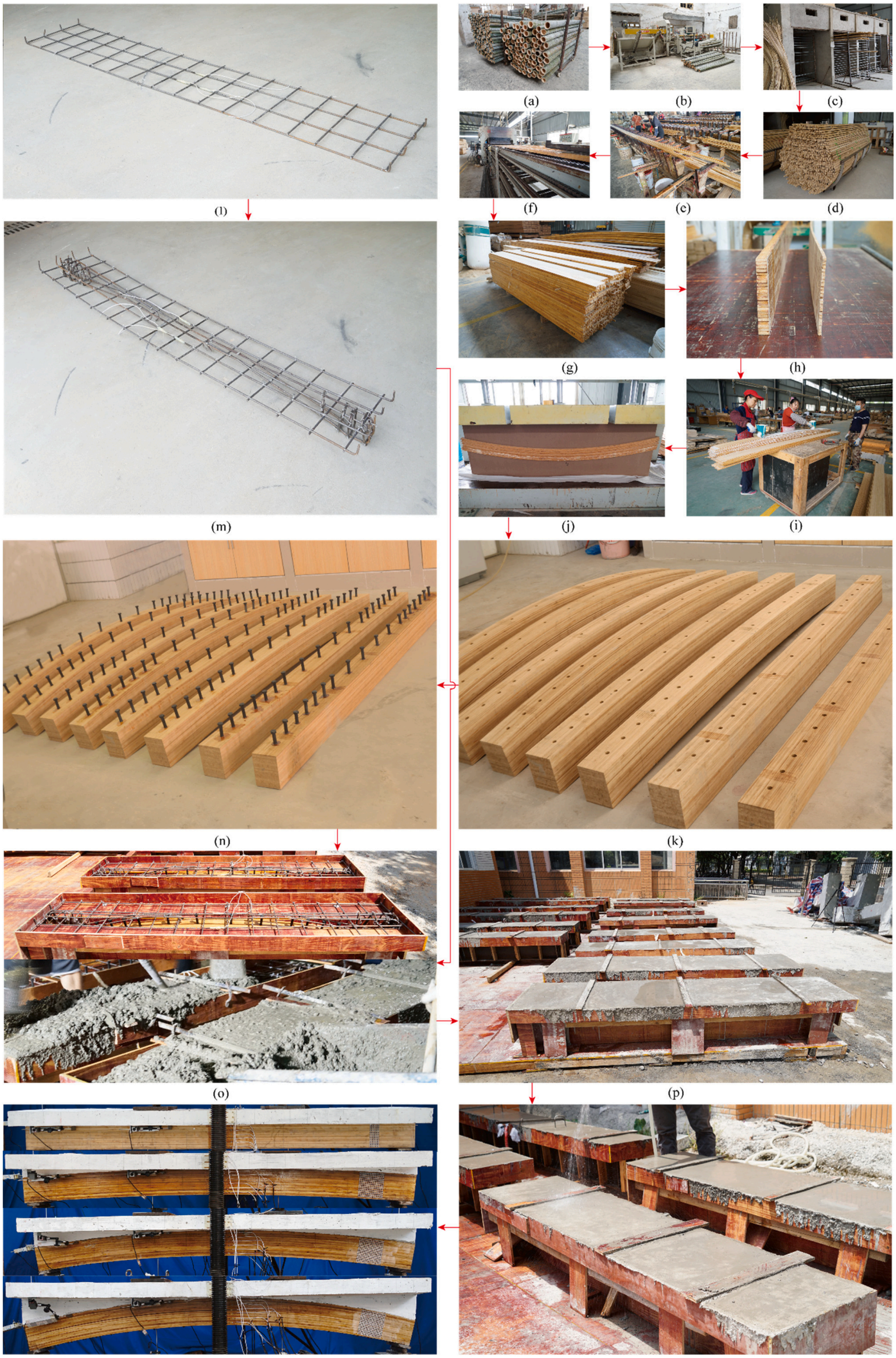

Fig. 4. Manufacturing process for LBC composite beams.

Table 2
Mechanical parameters of high strength bolt.

Type	Strength grade	Diameter [mm]	Tensile strength [MPa]	Yield strength [MPa]	Elastic modulus [MPa]
M16	8.8grade	16	838	670	2.0 × 105

cleaned with ethanol wipes before the fully mixed epoxy resin was poured into the pre-drilled hole, and the shear studs were then inserted. Extra caution was given to the amount of epoxy resin used for each hole to make sure the resin was fully filled to the top surface of the laminated bamboo. The completed components were cured in an indoor environment for two days (Fig. 4(k)) before making the mould for the later concrete casting.

2.2.3. Fabrication of the LBC composite beams

The detailed design of the reinforcement steel is specified in Fig. 3. All reinforce are HRB400 grade hot rolled ribbed bars [41]. As the flat top concrete plate was subjected to compression only, a nominal ϕ8 steel bar mesh @150 × 150 mm centre-to-centre was used to prevent the concrete from cracking prematurely (Fig. 4(l)). For the straight (BCC-0) and curved beams with 50 mm arch (BCC-1), no shear reinforcement was provided. For curved beams with 100 mm (BCC-2) and 150 mm (BCC-3) arch, shear reinforcement of ϕ8 @ 80 mm centre-to-centre was provided for the concrete insert between the bottom of the flat concrete plate to the top of the laminated bamboo component. A completed reinforcement wireframe is shown in Fig. 4(m).

After the reinforcement steel mesh and wireframe were fabricated, plywood concrete moulds were built around the two sides and the top of the laminated bamboo components. The sizes and distances between the inner surfaces of the concrete moulds were checked and braced with wooden bars to ensure the correct size of the concrete components once cast. The fabricated reinforcement steel mesh and wireframes were then laid into the concrete moulds, as shown in Fig. 4(n). The whole setup was then ready for the concrete casting.

Pre-mixed C30 [42] concrete was provided by a local commercial supplier, Liuzhou Yufeng Group Co. Ltd. The fresh concrete was vibrated during the casting to ensure that the pour was even and free of air bubbles (Fig. 4(o)). Nine concrete cubes were cast with the same concrete batch to validate the concrete's strength. After casting, the specimens were cured for 28 days (Fig. 4(p)). During this period, the specimens were moisturised regularly with sprayer to avoid excessive water loss in contact with the bamboo components.

3. Experimental process

3.1. Test setup

The flexural properties, as the key structural performance indicators of these eight beam specimens, were evaluated using the four-point bending test according to the Chinese Standard GB/T50329–2012 [43], which is comparable to BS EN 408 [44] for four-point bending test. A hydraulic loading system, YBD300–160, with a maximum capacity of 300 kN was used to apply the load. A load sensor, model BHR-4, with a measuring range of 0–300 kN was used. The total length of the specimens is 2420 mm from end to end, and the clear span between the centres of the supports is 2340 mm with a load spreading beam distributing two equal point loads at 780 mm apart. Before the actual four-point bending test, the specimens were pre-loaded with a small 20 kN force to confirm the equipment and sensor system's working condition and to eliminate poor contact and gaps within the test system. The loading rate was 1 mm/min with displacement control. Three LVDTs with a maximum measuring range of 100 mm were placed at the bottom surface of the mid-span, and the top surface of both end-supports to measure the maximum deflection of the beam, and to monitor the movement of the supports, respectively. Another 5 LVDTs (S1 – S5) with a maximum measuring range of 50 mm were installed in the left half of the specimen beam at equal intervals (except the external one, as shown in Fig. 5) along the bamboo-to-concrete interface to monitor the relative slippage of the bamboo-timber component and the performance of the shear studs. Foil strain gauges (BX120-100AA, gauge length is 100 mm) were fixed on the top and side surfaces of the mid-span section of the specimen beams to monitor the strain development at different loading stages. Details of the strain gauge layout are illustrated in Fig. 5(a). The actual test setup is shown in Fig. 5(b).

4. Test results and analysis

4.1. Failure mode

The key objectives of this study are to investigate the impact of the curvature on the failure modes of the LBC composite beams and to identify the differences in the structural behaviours between the straight and curved beams. After examining the features of eight specimen rupture tests, a total of seven failure modes were categorised (see Fig. 6) and the dominant failure mode and accompanying failure modes for each tested beam were identified. These failure modes are:

1. Shear-bonding failure of laminated bamboo (failure mode ①). This failure line is clearly developed along the glue line of the laminated bamboo and this behaviour indicates that bonding strength between the laminated bamboo layer is a weak point of this type of material.
2. Tension failure of the laminated bamboo component in the tension zone (failure mode ②). This is another failure mode associated with the laminated bamboo component (only two modes are associated with laminated bamboo).
3. Compression zone longitudinal cracks (full length) of the concrete slab (failure mode ③). This could be caused by the transverse bending moment from the load spreading plate at the top concrete surface, as there is no transverse tension steel at the top of the concrete surface.
4. Shear failure of concrete slab flanges at the shear-bending section of the composite beam (failure mode ④). This is a common failure mode observed at the final stage of the test.
5. Flexural cracks of the concrete slab in the pure bending section of the composite beam (failure mode ⑤). This happened to every specimen beam and the cracks distributed evenly within the pure bending section.
6. Diagonal shear cracks of the concrete inserts for specimens with large curvatures (BCC-2 and BCC-3, failure mode ⑥).
7. Interface shear slip failure between the laminated bamboo and concrete components (failure mode ⑦). This failure mode was observed for every specimen beam during the tests.

A complete record of the dominant and accompanying failure modes for each specimen is listed in Table 3 and more details are listed in the Appendix. The mechanical properties of laminated bamboo are shown in Table 4 and the design parameters of beam specimens are shown in Table 5.

For straight LBC beams (BCC-0a, b), all the dominant failure modes are the laminated bamboo glue line shear bonding failures (failure mode ①). The laminated bamboo in the tension zone was intact without sign of tension failure. All the other accompanying failure modes (failure mode ③, ④, ⑤ and ⑦) were not obvious until after the laminated bamboo's brittle dominant shear bonding failure. The shear bonding failures all happened abruptly with a distinctive large sudden sound, followed by the accompanying component failures.

The curved profile could be assumed to change the embed angle between the concrete and laminated bamboo, which could change the shear studs' effectiveness and eventually impact the failure modes. However, the test results reveal the opposite in that for all the curved

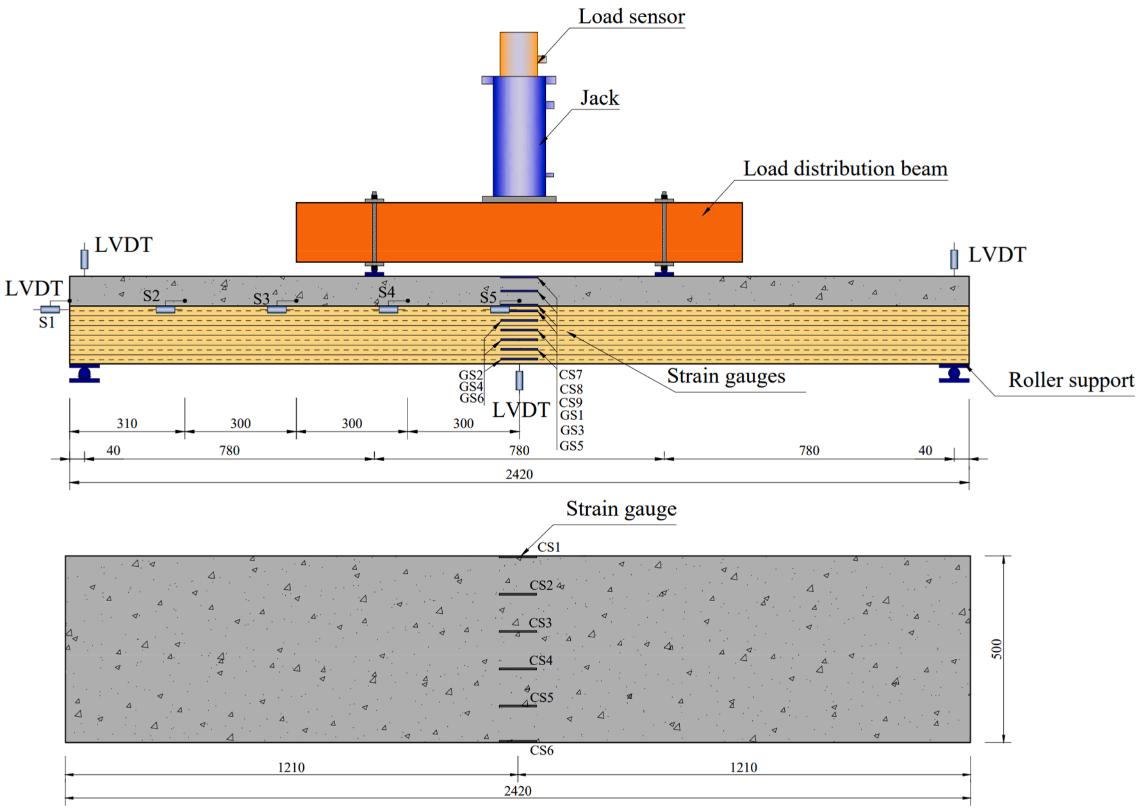

(a) Schematic drawing of the side and top views of the test setup with details of the strain gauge locations

(b) Actual test setup

Fig. 5. Test setup and strain gauge detail.

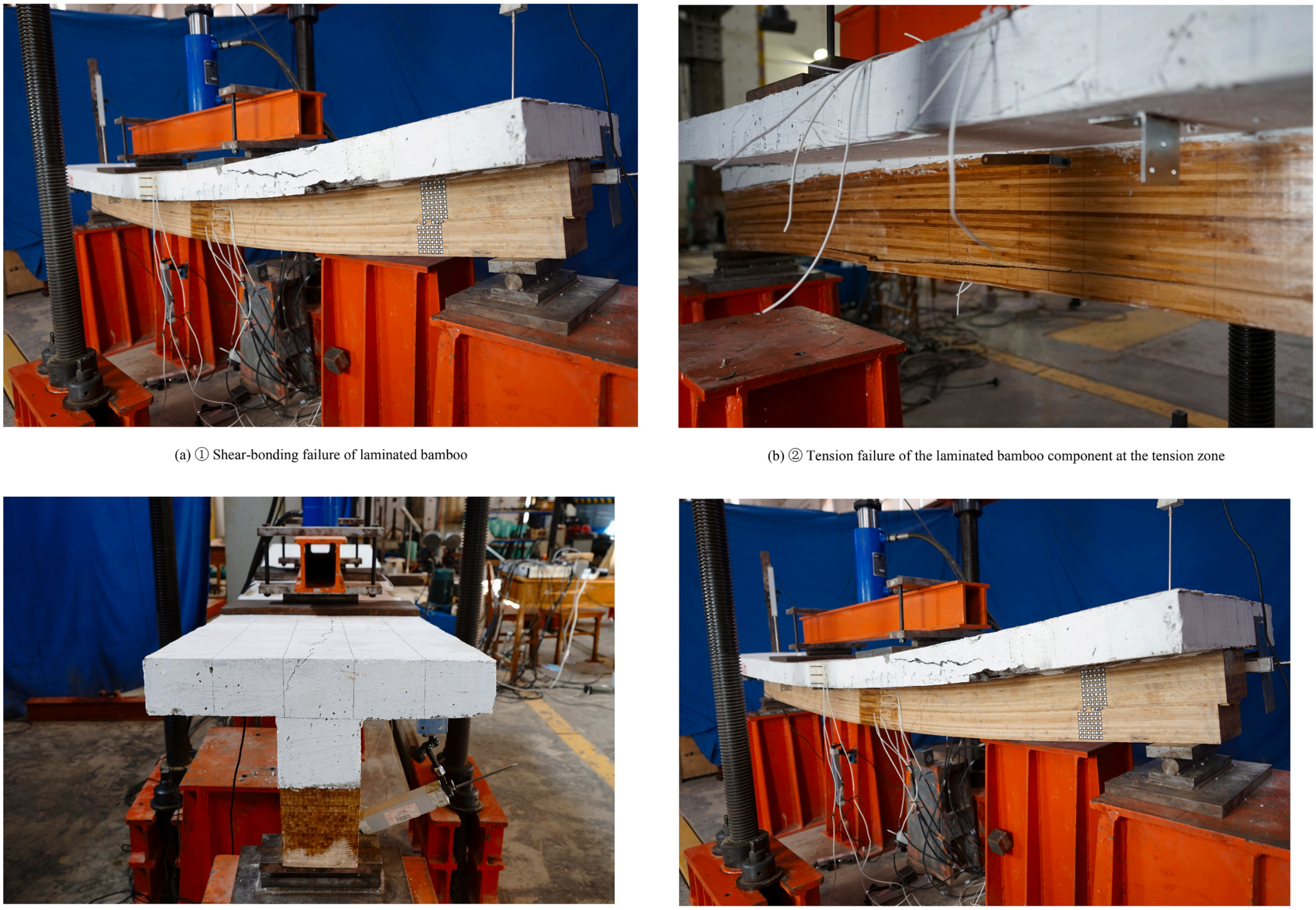

(a) ① Shear-bonding failure of laminated bamboo

(b) ② Tension failure of the laminated bamboo component at the tension zone

(c) ③ Compression zone longitudinal full-length crack(s) of the concrete slab

(d) ④ Shear failure of concrete slab flanges at shear-bending section of the composite beam

Fig. 6. Seven failure modes of LBC composite beams.

LBC beams (BCC-1a,b, BCC-2a,b, BCC-3a,b), even with different curvatures, the dominant failure modes are still the shear bonding failure (failure mode ①), the same as the straight beams. There was one new type of accompanying failure mode observed in the tests; failure mode ②, tension failure of the laminated bamboo component. This failure mode happened right after the dominant failure. Meanwhile, the straight beams experienced the damaging effect of the shock wave quite evenly distributed along the whole beam length at the instance of failure. The damaging effect of the shock wave was concentrated on the weakest mid-span section in the curved beams due to the uneven stiffness distribution along the beam length with curved profiles.

In conclusion, after comparing the structural behaviours between the straight and curved LBC composite beam, it is clear that there are two interacting key aspects that influence the structural behaviours of these beams. One is the effectiveness of the shear studs; another is the interlayer shear bonding strength of laminated bamboo components. The effectiveness of the shear studs reflects whether the concrete and laminated bamboo components are working together. The interlayer shear bonding strength of laminated bamboo is proven to be the thresholding parameter that determines the overall flexural strength of the whole composite beam, whether straight or curved. The weak interlayer shear bonding strength in the laminated bamboo component led to the consistent dominant failure mode in all the specimens. The development of a stronger laminated bamboo-composite would require further studies to improve the bonding strength of the adhesive and the fabrication technology to increase the shear bonding strength. The effectiveness of the shear studs is the key factor that ensures the composite synergy of the laminated bamboo and concrete components. When the shear studs yielded or failed, the two-part composite beam still worked as a semi-composite beam or two separated beams that stacked together. So, the overall stiffness is reduced and any further burden will be put on the shear bonding strength of the laminated bamboo component and cause an earlier failure in shear bonding. Thus, the effectiveness of the shear studs and the interlayer shear bonding strength of the laminated bamboo interact with each other.

Between these two key elements, the shear bonding strength is heavily reliant on the quality of the adhesive, for bonding the bamboo materials, and advanced fabrication technology. The latter falls slightly outside of structural engineers' key focus research areas but to improve the effectiveness of the shear studs is one of the most relevant structural engineering topics that attracted much research interest in the recent years [31,45–47] using the push-out test of scaled specimens. However, in this study, a different approach was developed to calibrate the concrete to laminated bamboo interface shear slip directly from the four-point bending test of full-scale LBC composite beams. Full details are discussed in Section 5.

4.2. Load-deflection behaviour and section stiffness

The load vs mid-span deflection curves for each specimen are shown in Fig. 7. To visualise the composite effect of these specimens, the boundaries of non-composite effect and full composite effect are shown

(e) ⑤ Flexural cracks of the concrete slab in the pure bending section of the composite beam

(f) ⑥ Diagonal shear cracks of the concrete inserts

(g) ⑦ Slippage failure between the laminated bamboo and concrete components

Fig. 6. (*continued*).

Table 3
Summary of the test result and failure modes.

Specimen	$P = 100$ kN			$\Delta = l/250$			Ultimate state			$P_{l/250}/P_{\max}$	Dominant failure mode	Accompanying failure modes
	Δ [mm]	Stiffness increase times	D_{eff}	$P_{L/250}$	Stiffness increase times	D_{eff}	$P_{\max}$	Increase times of $P_{\max}$	$\Delta_{\max}$ [mm]			
BCC-0a	15.11	100%	67.4%	75.2	100%	76.6%	210.0	100%	53.42	38%	①	③ + ⑤ + ⑦
BCC-0b	14.11			74.8			193.6				①	③ + ④ + ⑤ + ⑦
BCC-1a	11.27	119%	79.2%	97.2	124%	89.4%	224.2	94%	41.00	38%	① + ②	③ + ④ + ⑤ + ⑥ + ⑦
BCC-1b	13.57			87.4			154.4				①	⑤ + ⑦
BCC-2a	11.96	124%	82.5%	84.4	118%	86.6%	206.0	104%	50.08	50%	①	③ + ⑤ + ⑥ + ⑦
BCC-2b	11.66			91.2			212.3				① + ②	③ + ④ + ⑤ + ⑥ + ⑦
BCC-3a	12.79	122%	81.1%	87.2	118%	87.1%	208.3	96%	50.13	42%	①	⑤ + ⑥ + ⑦
BCC-3b	11.35			89.6			178.8				① + ②	④ + ⑤ + ⑥ + ⑦

Table 4
Mechanical properties from small clear laminated bamboo tests.

Type	Compressive Strength (Parallel to grain) [MPa]	Tensile strength (Parallel to grain) [MPa]	Bending strength [MPa]	Density [kg/m^3]	Elastic modulus [MPa]
Mean	53.5	91.1	107.4	630	8397
standard deviation	2.5	9.9	11.7	0.1	834.4
CoV [%]	4.5	10.8	10.9	0.81	9.9

Table 5
Parameters of beam specimens.

Specimen ID	Length of the beams [mm]	Cross-section of laminated bamboo beams/arches [mm]	Cross-section of concrete slab [mm]	Height of bamboo arch [mm]
BCC-0a, b	2420	120 × 156	500 × 80	0
BCC-1a, b	2420	120 × 156	500 × 80	50
BCC-2a, b	2420	120 × 156	500 × 80	100
BCC-3a, b	2420	120 × 156	500 × 80	150

as two slope-shaped straight boundary lines in the figures. The lower boundary corresponds to the non-composite effect (lower bound) scenario, i.e., assuming that the laminated bamboo and concrete components are simply stacked up with no shear transfer in between. The upper boundary corresponds to the full shear-bonded composite effect (upper bound), i.e., assuming that the laminated bamboo and concrete components are connected firmly without any interface slip. Another vertical dashed line in each figure marks the span/250 deflection limit, i.e., the equivalent service limited in deflection.

As shown in Fig. 7, the elastic section of the load-mid-span deflection curve is nearly the same and approximately linear for all groups of specimens until the maximum deflection reaches l/250 of the span. However, there is a noticeable difference between the curved and straight composite beams in the elastic stage. The curved composite beam demonstrated a better shear bonding effect than the straight ones. As shown in Fig. 7(b)-(d), the slope of the load-mid-span deflection curves for the curved composite beam at the elastic range is closer to the upper bound than the straight composite beam, as shown in Fig. 7(a). This result indicates that the curved laminated bamboo to concrete contact surface configuration has improved the composite effect in the elastic stage. The improvement in the curved composite beams could

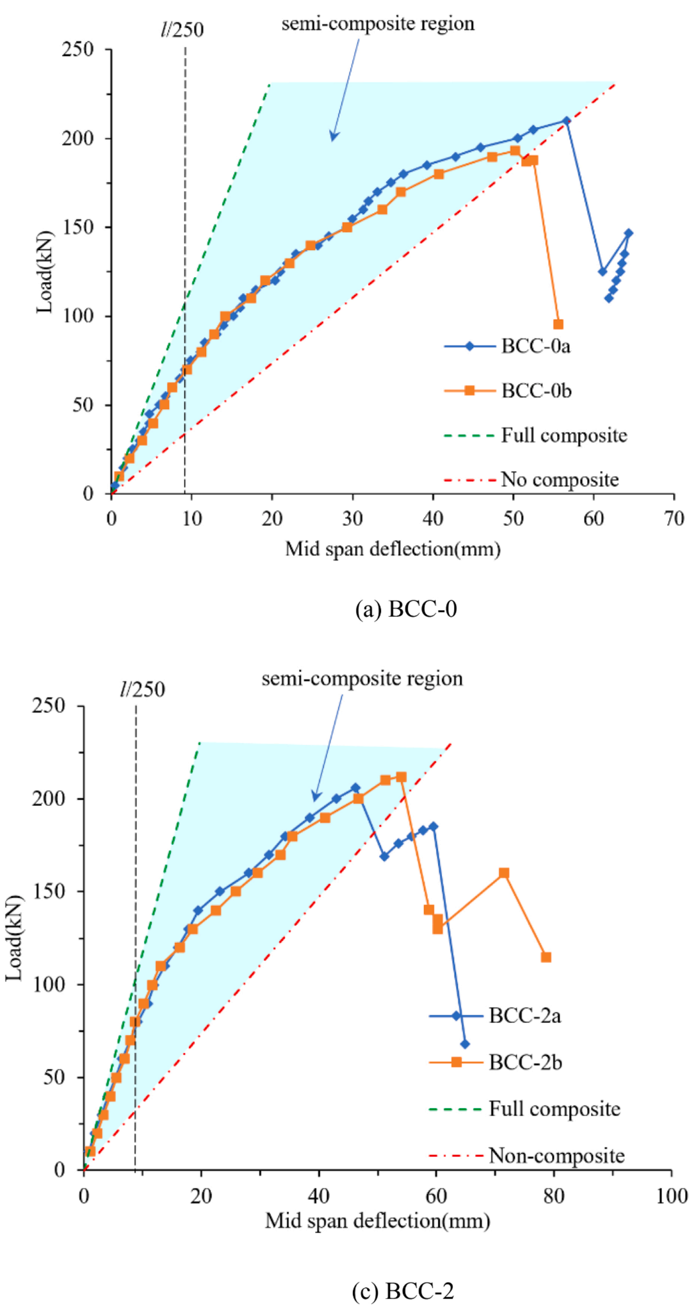

Fig. 7. Load-deflection curves of straight and curved LBC composite beams.

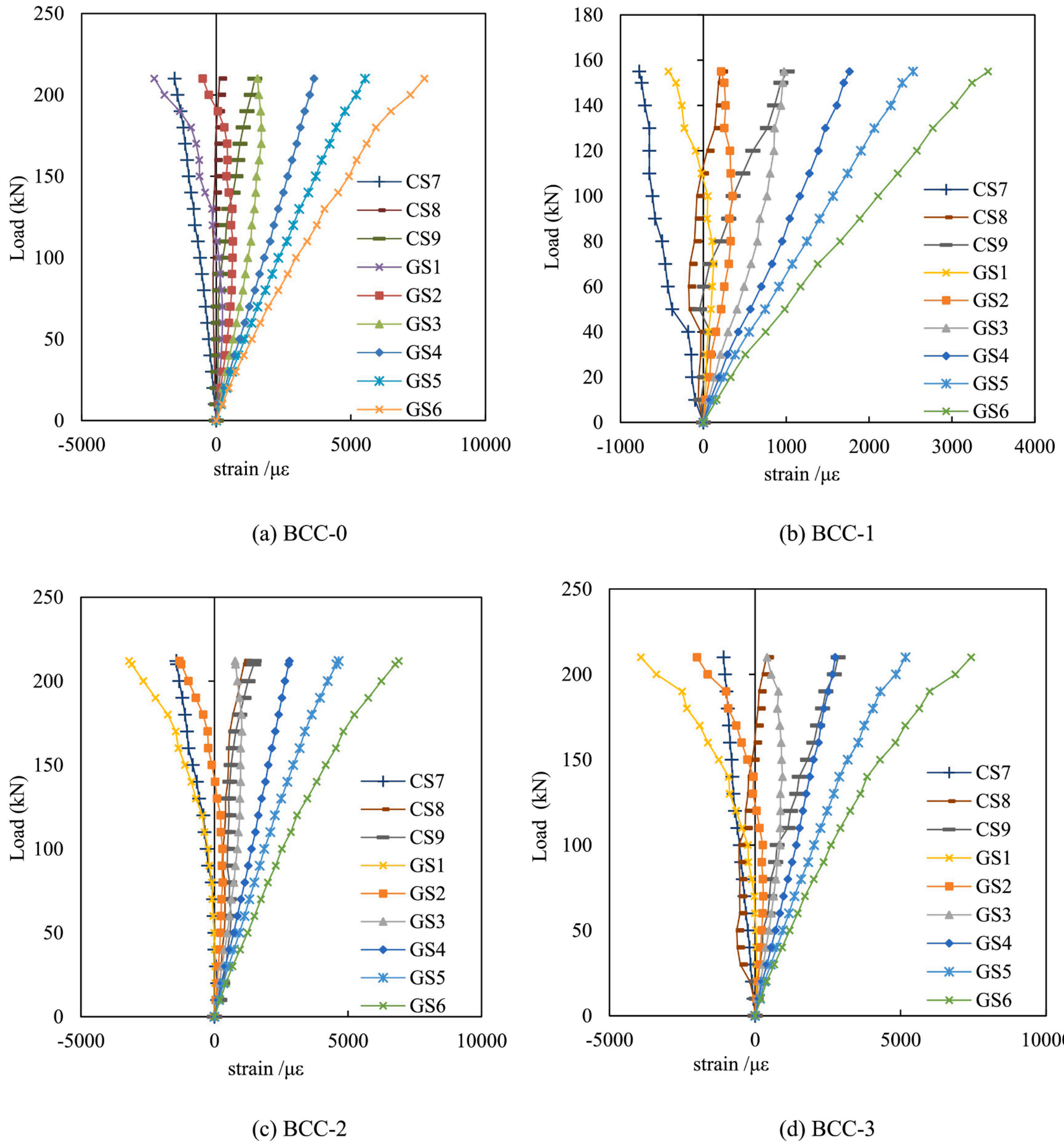

Fig. 8. Typical load-strain history curves of mid-span cross-section.

come from the varying angles of directions along which the shear studs were anchored into the concrete and laminated bamboo components. By varying the angle of the shear studs, a better interlocking mechanism can be formed between the concrete and laminated bamboo components. While the shear studs in the straight composite beams are parallel to each other without the benefit of forming the interlocking mechanism, the shear connecting effect is weaker than the curved beam. Another interesting observation is that all beams failed at or close to the lower bound line. This result indicates that the ultimate rupture occurred at the moment when the shear studs failed completely, i.e., there was no shear connection at all between the concrete and laminated bamboo contact surface.

The main test results for all specimens are summarised in Table 3. Three indicators are used to characterize the composite beam behaviour, two for the elastic stage and one for the inelastic stage. As there is no clear boundary between the elastic and inelastic stages, two indicators, one related to loading, i.e., loading at 100 kN, and one related to deflection, i.e., mid-span deflection reaches span/250, were used to mark the stage change after inspecting Fig. 7. The corresponding mid-span deflection at 100 kN and the corresponding load attainted at the moment the mid-span deflection reached span/250 were used to estimate the flexural stiffness and Coefficient of Composite Efficiency (CCE, D_{eff}) of the composite beams at the elastic stages. The CCE was used to specify the composite effect of the concrete and laminated bamboo components. It was quantified by the percentage of the fully composited beam stiffness that a specimen achieved in a test within the elastic range. The third component of Table 3 summarises the test results for the ultimate state, including ultimate loads, maximum mid-span deflections, and the ductility indicator. The ductility is the ratio of the corresponding load $P_{l/250}$ (loading attainted when mid-span deflection reached span/250) to the ultimate load.

As shown in Table 3, in the elastic range, the overall flexural stiffness increased by around 20%, and the average CCE increased from 67 to 77% to 80–90% when compared with the straight composite beam, whether using the 100 kN load or span/250 as the phase change indicator. However, the test results also show that the flexural stiffness and CCE of the composite beams did not increase when the curvature increased, they either levelled off or slightly decreased. For the ultimate

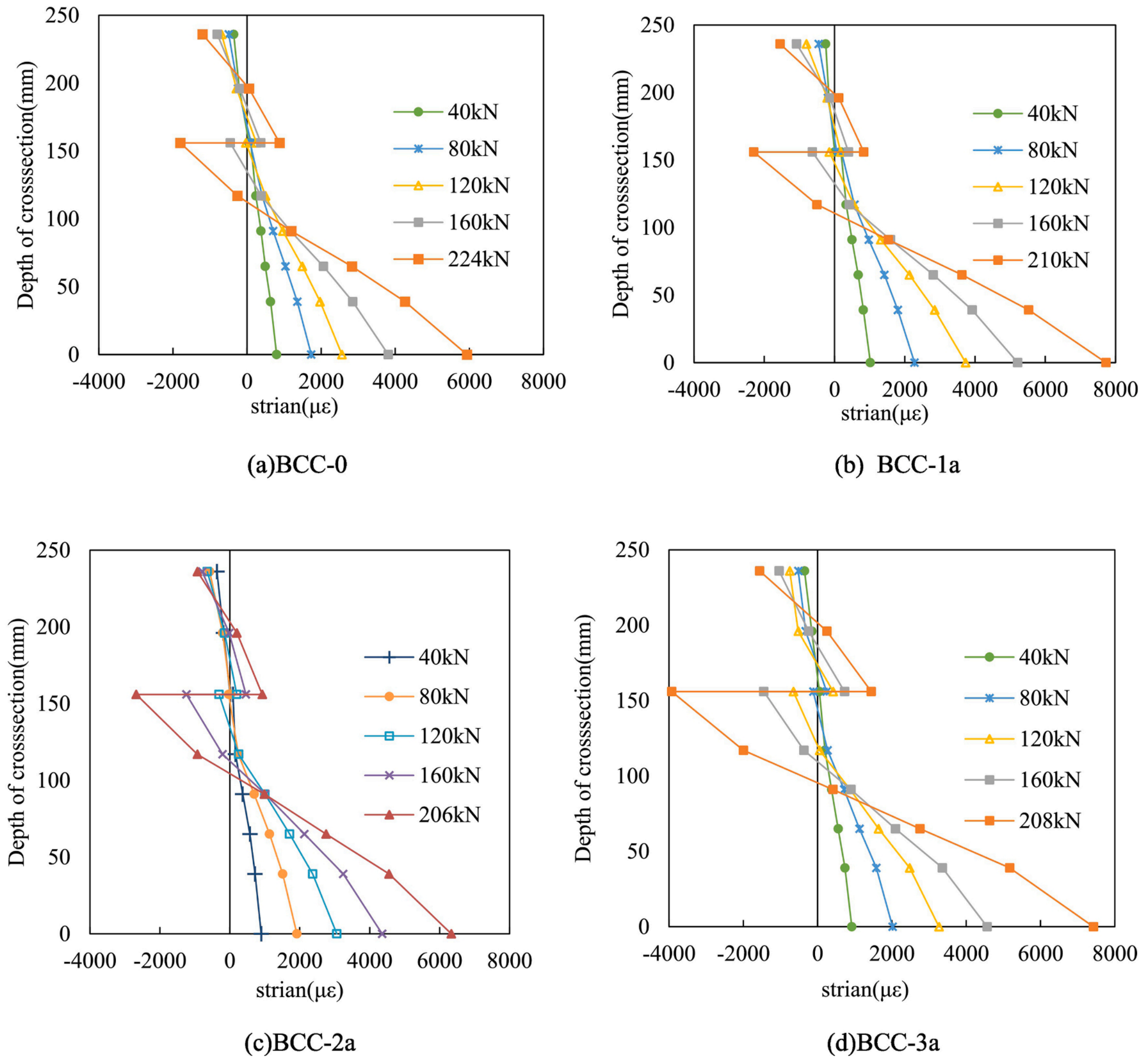

Fig. 9. Strain distributions of mid-span cross-section at different loads.

limit state, there is no noticeable increase in the ultimate loads and maximum deflections recorded from the straight to curved composite beams. However, the ductility of the composite beams with a medium level of curvature shows a slight increase when compared to the straight, low, and high-curvature composite beams. In conclusion, the curved LBC composite beams have a slightly higher flexural stiffness in the elastic stage when compared to the straight LBC beams, but the curved design setup does not benefit from the ultimate flexural capacity. There is no clear benefit to the ductility of the composite beams except a small increase for the medium curvature composite beams.

4.3. Load-strain relationship

The load-strain relationship of the mid-span cross-section was measured by the strain gauges distributed vertically on the side surface (CS7–9 on concrete, GS1–6 on laminated bamboo, as shown in Fig. 5). The load-strain history logged by the sensors are shown in Fig. 8. Compared to the other non-bio-based composite beams, such as steel reinforced concrete (SRC) beams, the tracks in the strain history plot intersect each other. For example, the tracks of strain gauges CS7–9 and GS1–3 intersect. This result indicates that there was interface shear slip between the concrete and the laminated bamboo contact surface and the shear connectors were degrading during the test. To verify this degradation, the load-strain histories were re-plotted along the depth of the cross-section, as shown in Fig. 9. When subjected to small loading, the strain profile along the depth of the cross-section suggests that the cross-section more and less remained plane. However, when the loading increased, the difference between the strain gauges CS9 and GS1, next to the concrete to laminated bamboo contact surface, also increased due to the shear connector degrading and shear stud failures. So at this stage, the plane cross-section remained plane regionly, i.e., the plane of concrete and laminated bamboo components remained two separated planes, respectively. The LVDTs S1–5 also captured the slip between the concrete and laminated bamboo, and the test results are shown in Fig. 10.

The load-strain history of strain gauge CS1–6, installed at the top surface of the mid-span of the concrete component, is shown in Fig. 11. Most of the readings from different sensors were well aligned, i.e., there was no significant twist during the test. But some sensors at the cross-section's edge exhibited a discernible, but insignificant, discrepancy with others. This indicates the specimen was slightly twisted during the test which could be due to the imperfect test setup. This observation suggests that using strain gauges at the top surface of a T-section at mid-span is a reliable way to monitor whether a lateral torsion developed during the test.

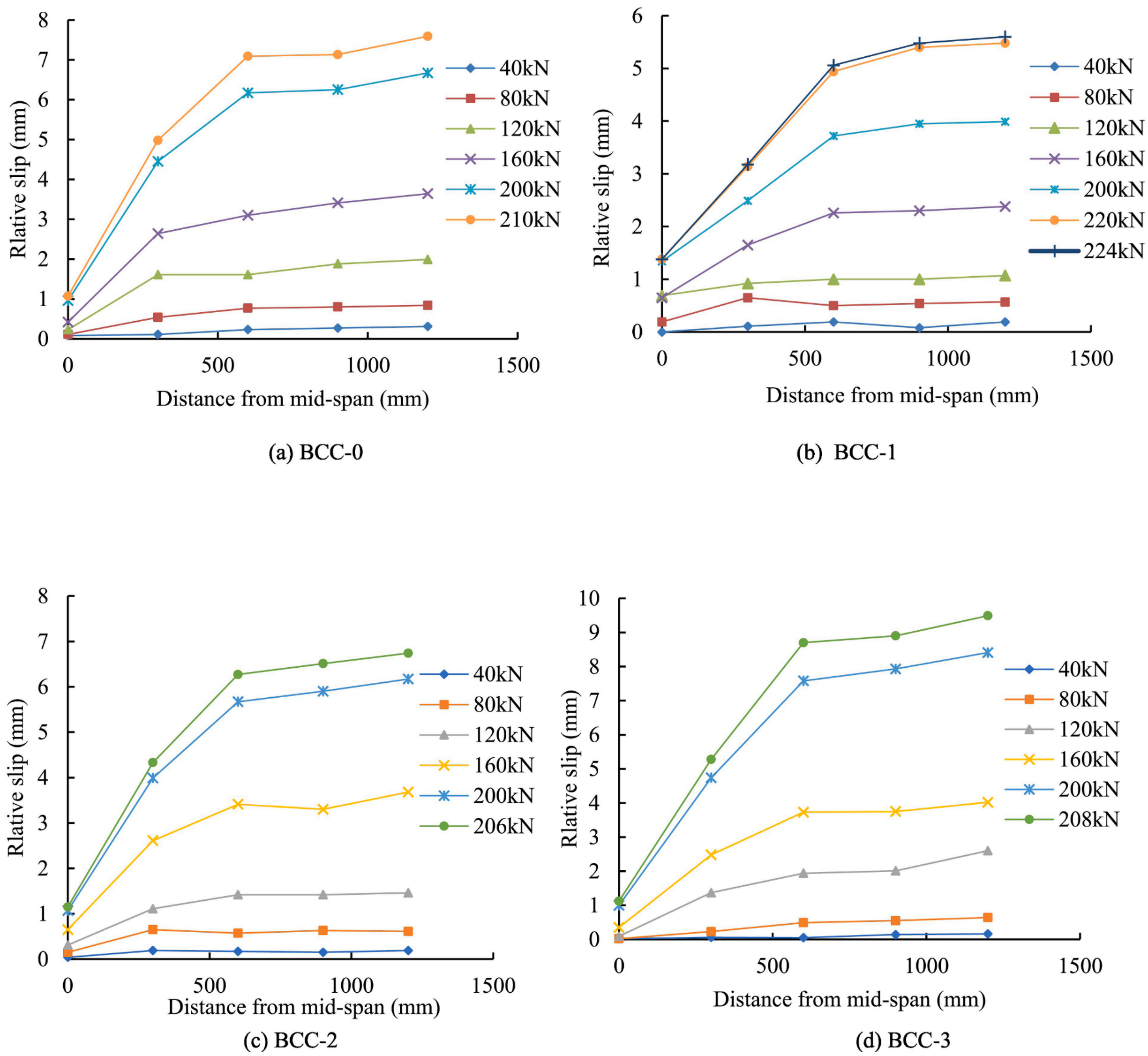

Fig. 10. Longitudinal slip distribution at different loads.

5. Calibration of interface shear slip with strain gauge validation

In small specimen push-out tests, the real stress status in a full-scale TCC or LBC beams may not be accurately replicated during the tests. The results from small shear push-out test are also difficult to apply to analytical models, such as the spring-rigid block analogy. Another more sensible method to calibrate the load-interface slip is to directly measure the load-interface slip in full-scale structural member tests, such as the four-point bending test. The interface slip should be measured at positions next to the interface surface. The measured slip can reflect the behaviour of the shear connector in real structures rather than in the small push-out specimens. For example, in a four-point bending test, within the pure bending section, in theory, there should be no shear force between the concrete and laminated bamboo. Hence there should be no slip between the concrete and laminated bamboo interface. However, due to the shear slip at the shear-bending sections, the shear force along the interface will gradually transfer into the pure bending section and be shared by the shear connectors in this section. It is hard to simulate this type of flange-to-web interface structural internal interaction using the push-out test, thus it is hard to utilise the push-out model to predict the real structural behaviour. Monitoring the interface slip from the mid-span of the beam to the end of the beam (or close to the end to avoid the end effect) in a four-point bending test can capture this effect. If this method of calibration is accurate, it will also pave the way for the development of a nonlinear model for interface shear slip for TCC or LBC beams that consider the flange-to-web interface interaction. To prove the accuracy of the proposed method, the interface shear slips measured were validated by the strain gauge measurement for each sample.

The difference between the readings of LVDT S2 and S5 (position specified in Fig. 5) was selected to quantify the average slippage between the laminated bamboo and concrete. S1 was not used to prevent the potential end effects from disrupting the regular pattern that the middle span may have. S3, S4, and S5 were also not selected to avoid measurement on a short distance with a small number of shear studs in between. Such that an irregular transducer reading of an incremental step of a single shear stud failure would not distort the record of the regular pattern of shear bonding failure at the element level. After obtaining the average interface shear slip between the positions of LVDT S2 and S5, the corresponding longitudinal strain difference can be calculated by:

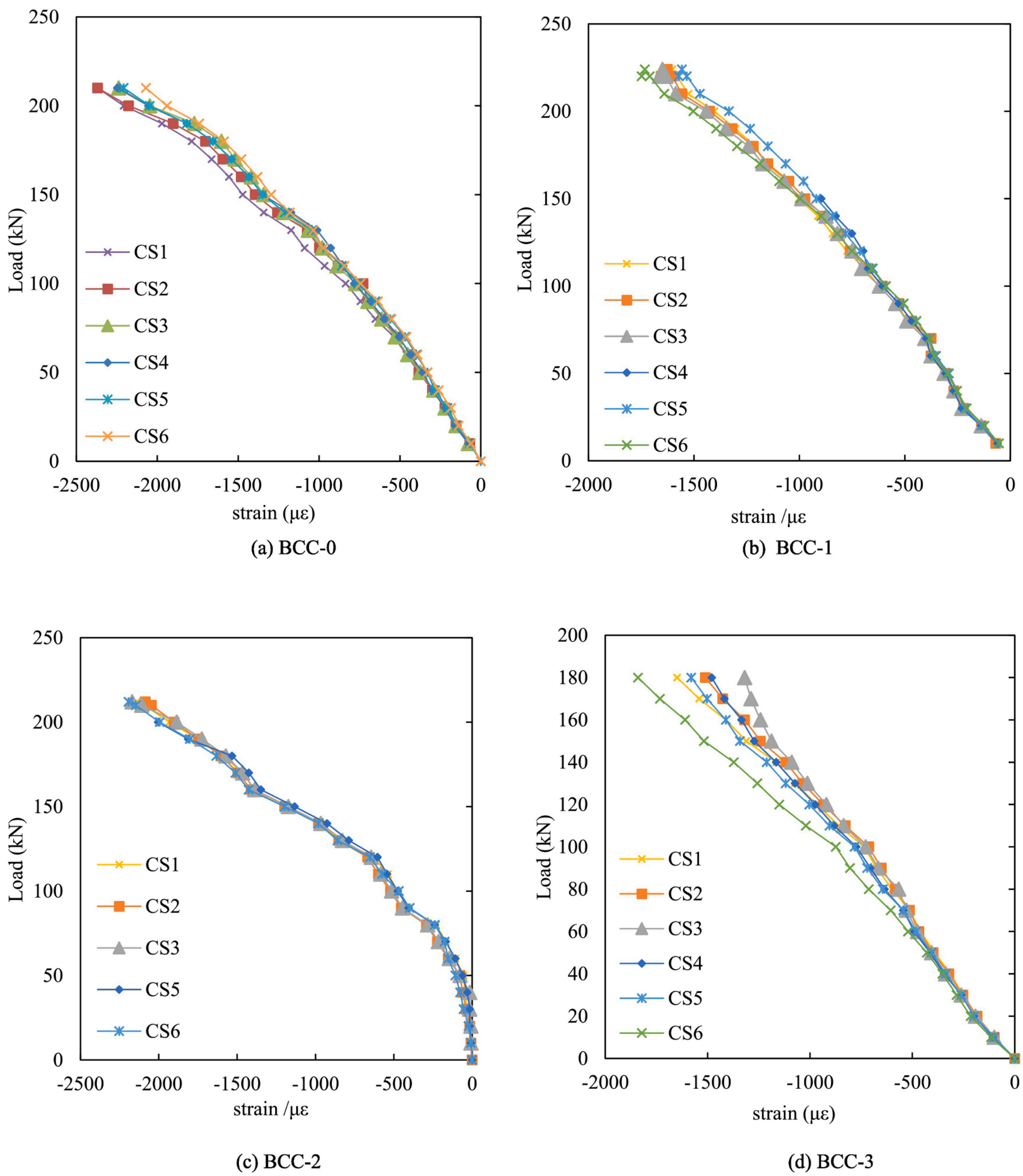

Fig. 11. Load-strain history at top surface of the concrete component.

$$\varepsilon_{S2-S5} = \frac{\delta_{S2-S5}}{L_{S2-S5}} \tag{1}$$

where, ε_{S2-S5} is the strain difference at the longitudinal direction, δ_{S2-S5} is the average interface shear slip measured the LVDT S2 and S5, L_{S2-S5} is the distance between the LVDT S2 and S5, which is 900 mm in this study.

This strain difference measured by the LVDTs is the critical parameter for constructing the nonlinear shear connection model between the concrete and laminated bamboo components. Hence, this parameter shall be validated by another type of sensor system. This study proposes a strain gauge-based measuring system to validate the LVDT measurements, considering that the concrete to laminated bamboo surface was not glued together but instead connected by the shear studs. When the shear studs gradually failed in a group, without the contact constrained by gluing, the strains at contact surfaces within each component tended to even out themselves. So, the strain difference of both surfaces, measured by strain gauges CS9 and GS1 (as shown in Fig. 5), should reflect the average strain difference calculated from the interface shear slip measured by LVDT S2 and S5. The comparison of results from the two measuring systems are shown in Fig. 12 (a)-(h). The results reveal that the interface slip is developed nonlinearly, and the non-linearity started from the very early stage of the test. The results also suggest a strong correlation between the LVDT and strain gauge measurements, thus, the interface shear slip measured by the LVDT is reliable and is crucial for developing the nonlinear block spring model for LBC composite beams. The test results for each type of specimen beam shown in Fig. 12 can also group together and fit a polynomial curve to predict the load-to-strain difference, as shown in Fig. 13. Another advantage of the proposed interface shear slip calibration method is that it can be applied not only to shear stud connections but also to other types of shear connectors such as screws, shear plates, etc.

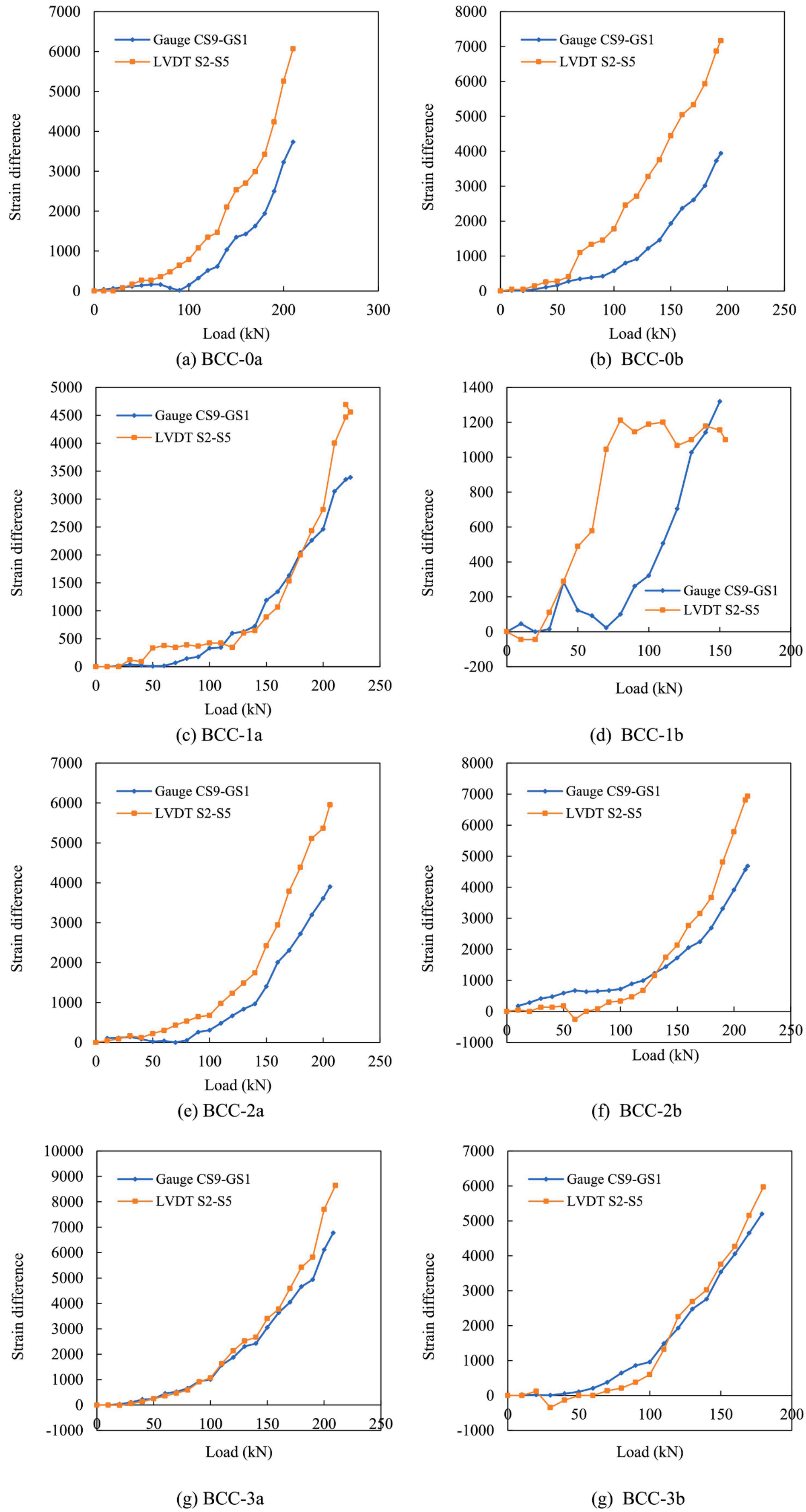

Fig. 12. Strain difference at concrete to laminated bamboo surface measured by strain gauge and LVDT.

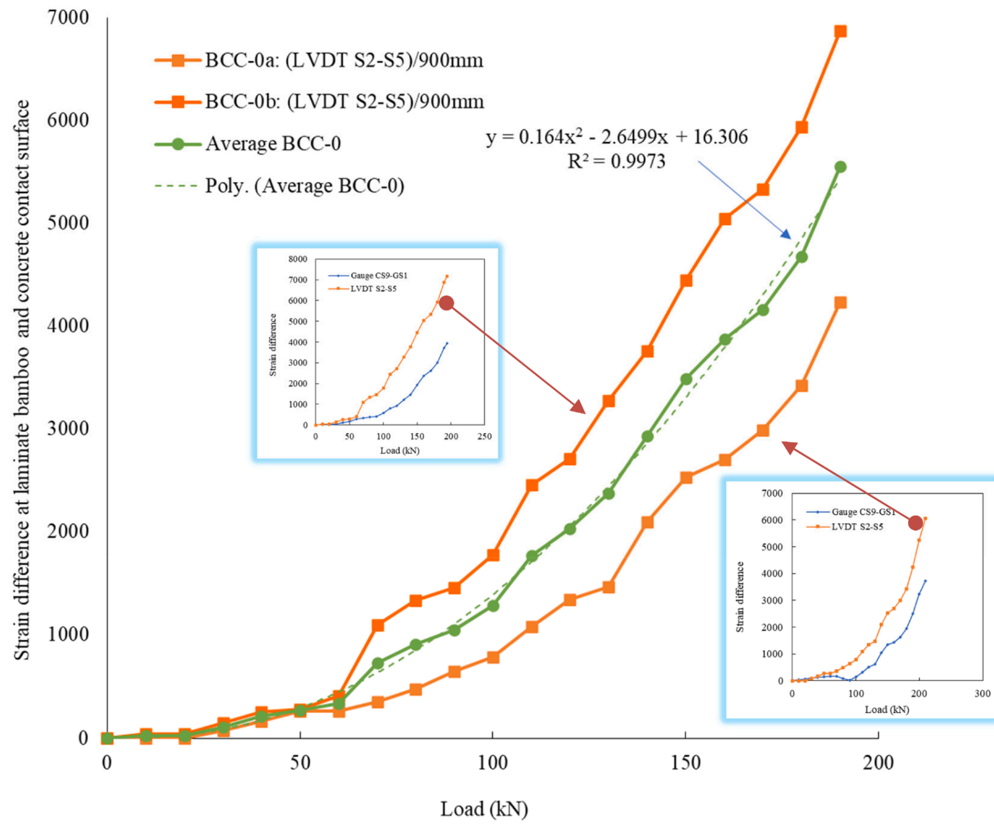

Fig. 13. Curve fitting for load to strain difference relationship.

6. Conclusions

This study experimentally investigated and compared the structural performance of the curved and straight LBC beams, including the failure modes, flexural properties, and strain distribution during the four-point bending loads, aiming to provide practical guidance for improving the manufacturing and design of the LBC beams. Based on the test results, a novel flange-to-web interface shear slip calibration method was proposed. The interface shear slip is calibrated at the structural member level with the displacement transducer measurements along the concrete to laminated bamboo interface. The interface slips were validated with the mounted strain gauges for each specimen. The following key conclusions are drawn based on the outcome of this study:

1) The interlayer shear bonding strength of laminated bamboo is proven to be the thresholding parameter that determines the overall flexural strength of the whole composite beam, whether straight or curved. The weak interlayer shear bonding strength in the laminated bamboo component led to the consistent dominant failure mode in all the specimens.
2) The effectiveness of the shear studs interacts with the interlayer shear bonding strength of the laminated bamboo component. Failure of the interface shear connections will accelerate the laminated bamboo shear failure.
3) The test results also suggested that the curved LBC composite beams have a slightly higher flexural stiffness in the elastic stage when compared to the straight LBC beams. Yet, the curved design setup does not benefit the ultimate flexural capacity. There is no clear benefit to the ductility of the composite beams except a small increase for the medium curvature composite beams.
4) The proposed flange-to-web interface shear slip calibration method is proven to effectively calibrate the interface slip and longitudinal after-slip strain redistribution, which was validated by the stain gauge measurement. The method can be extended to other types of shear connectors, such as screws, shear plates, etc.

Declaration of Competing Interest

The authors declare that they have no known competing financial interests or personal relationships that could have appeared to influence the work reported in this paper.

Data availability

No data was used for the research described in the article.

Acknowledgements

This research was supported/partially supported by the Royal Academy of Engineering-Industrial Fellowship (IF\192023), National Natural Science Foundation of China (51768008, 52168016), British Council and Ministry of Education, China (UK-China-BRI Countries Education Partnership Initiative 2019), British Council (Enabling Grants to Strengthen UK-China Institutional Partnerships through academic collaboration 2021), Natural Science Foundation of Guangxi Zhuang Autonomous Region (2019JJA160137), and Royal Academy of Engineering-Visiting Professor (VP2021\7\12). The authors also would like to express their special gratitude to the significant investment from the Research, Innovation & Enterprise office of Edinburgh Napier University that enable us to acquire industrial level of press machine to support this research project.

Appendix A

Specimen ID	Failure testing beams	Dominant failure modes (marked in white)	Accompanying failure modes (marked in blue)
BCC-0b	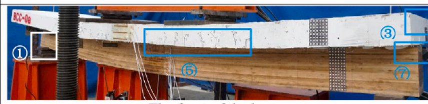 The front of the beam	 ①	 ③ ⑤ ⑦
BCC-0b	 The front of the beam	 ①	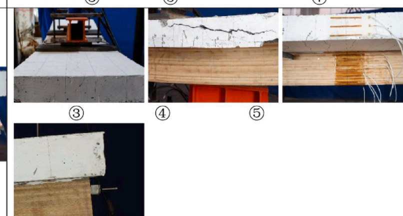 ③ ④ ⑤ ⑦
BCC-1a	 The back of the beam 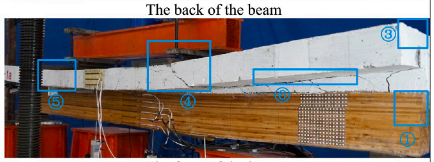 The front of the beam	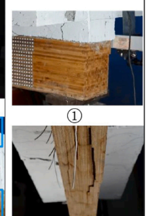 ① ②	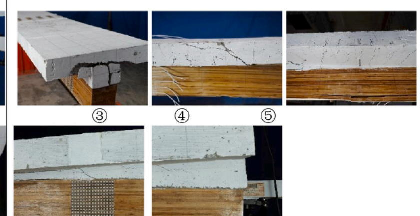 ③ ④ ⑤ ⑥ ⑦
BCC-1b	 The front of the beam	 ①	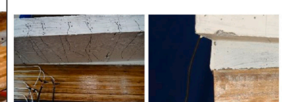 ⑤ ⑦
BCC-2a	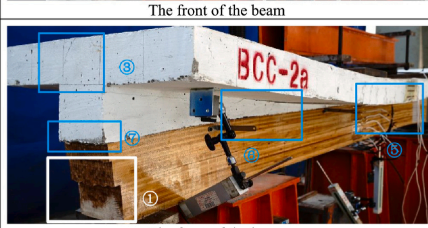 The front of the beam	 ①	 ③ ⑤ ⑥ ⑦
BCC-2b	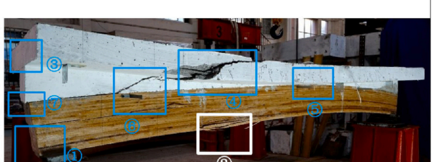 The back of the beam	 ① ②	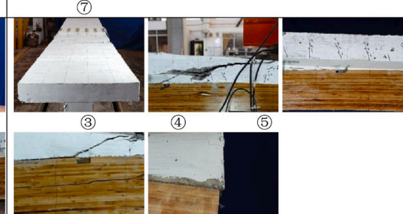 ③ ④ ⑤ ⑥ ⑦
BCC-3a	 The front of the beam	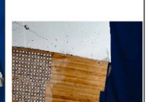 ①	 ⑤ ⑥ ⑦
BCC-3b	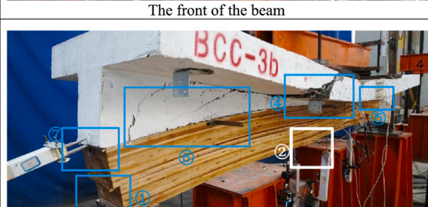 The front of the beam	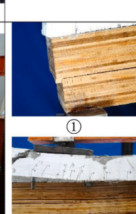 ① ②	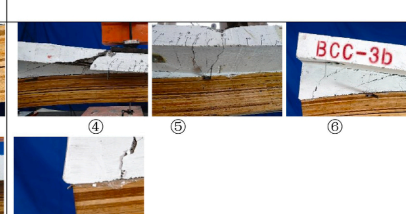 ④ ⑤ ⑥ ⑦

References

[1] Ogrin A, Hozjan T. Timber-concrete composite structural elements. In: Engineered Wood Products for Construction. IntechOpen; 2021.
[2] Van der Linden ML. Timber-Concrete Composite Beams Heron-English Edition44; 1999. p. 215–36.
[3] Khorsandnia N, Valipour H, Schänzlin J, Crews K. Experimental investigations of deconstructable timber–concrete composite beams. J Struct Eng 2016;142:04016130.
[4] Hadigheh SA, McDougall R, Wiseman C, Reid L. Evaluation of composite action in cross laminated timber-concrete composite beams with CFRP reinforcing bar and plate connectors using digital image correlation (DIC). Eng Struct 2021;232:111791.
[5] Thai M-V, Elachachi SM, Ménard S, Galimard P. Vibrational behavior of cross-laminated timber-concrete composite beams using notched connectors. Eng Struct 2021;249:113309.
[6] Frohnmüller J, Fischer J, Seim W. Full-scale testing of adhesively bonded timber-concrete composite beams. Mater Struct 2021;54:187.
[7] Khorsandnia N, Valipour H, Bradford M. Deconstructable timber-concrete composite beams with panelised slabs: finite element analysis. Constr Build Mater 2018;163:798–811.
[8] Gharavi N, Zhang H, Xie Y, He T. End effect on determining shear modulus of timber beams in torsion tests. Constr Build Mater 2018;164:442–50.
[9] Gharavi N, Zhang H. Study on the impact of size and position of the shear field in determining the shear Modulus of glulam beam using photogrammetry approach. Int J Struct Construct Eng 2018;12:218–22.
[10] Mohamed A, Deng Y, Zhang H, Wong SHF, Uheida K, Zhang YX, et al. Photogrammetric evaluation of shear modulus of glulam timber using torsion test method and dual stereo vision system. Eur J Wood Wood Prod 2021; 79:1209-1223.
[11] Mohamed A, Uheida K, Quan Y, Zhang H. Applicability of the torsion test and photogrammetric approach on structural timber beams. Int Wood Prod J 2021:1–12.
[12] Mohamed A, Uheida K, Quan Y, Zhang H. Verification of the photogrammetric approach on the torsion test method for timber beams. Int Wood Prod J 2022;13:3–14.
[13] Zhao K, Wei Y, Yan S, Chen S, Dong F. Experimental and analytical investigations on flexural behavior of bamboo beams strengthened with steel bars. Adv Struct Eng 2021;24:3338–56.
[14] Zhao K, Wei Y, Chen S, Hang C, Zhao K. Experimental investigation of the long-term behavior of reconstituted bamboo beams with various loading levels. J Build Eng 2021;36:102107.
[15] Zhang H, Gharavi N, Wong SHF, Deng Y, Bahadori-Jahromi A, Limkatanyu S, et al. Effect of concentrated butt-joints on flexural properties of laminated bamboo-timber flitch beams. J Sandw Struct Mater 2021;24(2):1226–44.
[16] Li X, Li L, Li N, Bao M, Bao Y, Wu Z, et al. Sustainable production of engineered bamboo scrimber composites for construction and flooring applications. Constr Build Mater 2022;347:128615.
[17] Fahim M, Haris M, Khan W, Zaman S. Bamboo as a construction material: prospects and challenges. Adv Sci Technol Res J 2022;16:165–75.
[18] Li H, Zhang H, Qiu Z, Su J, Wei D, Lorenzo R, et al. Mechanical properties and stress strain relationship models for bamboo Scrimber. J Renewable Mater 2020:8.
[19] Cassandra A. Bamboo Architecture and Construction with Osca Hidalgo. 2009.
[20] Wang Z, Wei Y, Li N, Zhao K, Ding M. Flexural behavior of bamboo–concrete composite beams with perforated steel plate connections. J Wood Sci 2020;66:4.
[21] Wang Z, Wei Y, Hu Y, Chen S, Zhao K. An investigation of the flexural performance of bamboo-concrete composite beams with precast light concrete slabs and dowel connectors. J Build Eng 2021;41:102759.
[22] Tesfaye Deresa S, Xu J, Shan B, Ren H, Xiao Y. Experimental investigation on flexural behavior of full-scale glued laminated bamboo (glubam)-concrete composite beams: A case study of using recycled concrete aggregates. Eng Struct 2021;233:111896.
[23] Duan Y, Zhang J, Tong K, Wu P, Li Y. The effect of interfacial slip on the flexural behavior of steel-bamboo composite beams. Structures. 2021;32:2060–72.
[24] Shan B, Li TY, Deng JY, Zou Y, Xiao Y, Yu Q, et al. Experimental research on novel RPC-steel composite connections for prefabricated glubam-concrete composite beams. Constr Build Mater 2022;333:127397.
[25] Xu JJ, Xiong WW, Shan B, Wen J, Xiao Y. Bending stiffness of bamboo-concrete composite (BCC) beams under short-term loads. J Build Eng 2022;60:105170.
[26] Deresa ST, Xu J, Demartino C, Minafò G, Camarda G. Static performances of timber-and bamboo-concrete composite beams: A critical review of experimental results. Open Construct Build Technol J 2021:15.
[27] Crocetti R, Sartori T, Tomasi R. Innovative timber-concrete composite structures with prefabricated FRC slabs. J Struct Eng 2015;141:04014224.
[28] Denouw DD, Messan A, Fournely E, Bouchair A. Influence of interlayer in timber-concrete composite structures with threaded rebar as shear connector-experimental study. Am J Civil Eng Architect 2018;6:38–45.
[29] Lukaszewska E, Johnsson H, Fragiacomo M. Performance of connections for prefabricated timber–concrete composite floors. Mater Struct 2008;41:1533–50.
[30] Du H, Hu X, Sun Z, Fu W. Shear stiffness of inclined screws in timber–concrete composite beam with timber board interlayer. Adv Struct Eng 2020;23:3555–65.
[31] Wei Y, Wang Z, Chen S, Zhao K, Zheng K. Structural behavior of prefabricated bamboo-lightweight concrete composite beams with perforated steel plate connectors. Archiv Civil Mech Eng 2021;21:15.
[32] Fragiacomo M, Gutkowski RM, Balogh J, Fast RS. Long-term behaviour of wood-concrete composite beams with notched connection detail. 2006.
[33] Ceccotti A. Composite concrete-timber structures. Prog Struct Eng Mater 2002;4:264–75.
[34] Oudjene M, Meghlat EM, Ait-Aider H, Lardeur P, Khelifa M, Batoz JL. Finite element modelling of the nonlinear load-slip behaviour of full-scale timber-to-concrete composite T-shaped beams. Compos Struct 2018;196:117–26.
[35] Zhang L, Zhou J, Chui Ying H, Tomlinson D. Experimental investigation on the structural performance of mass timber panel-concrete composite floors with notched connections. J Struct Eng 2022;148:04021249.
[36] Pleskov PF. Teorija rasceta derevjannych sostavnych sterznej: Gosstrojizdat. 1952.
[37] Smith I. Series type solutions for built-up timber beams with semi-rigid connections. Proc Inst Civ Eng 1980;69:707–19.
[38] Smith I. Analysis of plywood stressed skin panels with rigid or semi rigid connections. In: Research Report TRADA (UK). no 1/79; 1979.
[39] Latham CT, Toledano A, Murakami H, Seible F. A shear-deformable two-layer plate element with interlayer slip. Int J Numer Methods Eng 1988;26:1769–89.
[40] JGJ 82—2011. Strength Bolted connections technical regulations. Chinese Standard; 2011.
[41] GB1499.2—2007. Steel for the reinforcement of concrete – Part 2: Hot rolled ribbed bars. Chinese Standard; 2007.
[42] GB/T 50107—2010. Standard for evaluation of concrete compressive strength. Chinese Standard; 2010.
[43] Urban MoHa. GB/T 50329-2012 standard for test methods of timber structures. Chinese Standard; 2012.
[44] BSI. BS EN 408: 2010+ A1. Timber structures Structural timber and glued laminated timber Determination of some physical and mechanical properties. British Standard Institute; 2012. p. 2012.
[45] Zhang X, Xuan L, Huang W, Yuan L, Li P. Structural design and analysis for a timber-concrete hybrid building. Front Mater 2022:9.
[46] Auclair SC, Sorelli L, Salenikovich A. A new composite connector for timber-concrete composite structures. Constr Build Mater 2016;112:84–92.
[47] Ling Z, Zhang H, Mu Q, Xiang Z, Zhang L, Zheng W. Shear performance of assembled shear connectors for timber–concrete composite beams. Constr Build Mater 2022;329:127158.
[48] Zhang L, Zhou J, Zhang S, Chui YH. Bending stiffness prediction to mass timber panel-concrete composite floors with notched connections. Eng Struct 2022;262:114354.